Semi-microscopic folding model for the description of two-body halo nuclei

J. A. Lay,* A. M. Moro,† and J. M. Arias‡
Departamento de FAMN, Facultad de Física, Universidad de Sevilla, Apartado 1065, E-41080 Sevilla, Spain

Y. Kanada-En'yo§
Yukawa Institute for Theoretical Physics, Kyoto University, Kyoto 606-8502, Japan
(Received 4 November 2013; published 31 January 2014)

One-neutron halo nuclei, composed of a weakly bound particle coupled to a *core* nucleus, are studied within a particle-plus-*core* model. A semi-microscopic method to generate the two-body Hamiltonian of such a system, including core excitation, is proposed. The method consists of generating the spin-independent part of the valence-*core* interaction using a single-folding procedure, convoluting a realistic nucleon-nucleon (NN) interaction with the core transition densities. The latter are calculated with the antisymetrized molecular dynamics (AMD) method. The prescription is applied to the well known halo nucleus, ^{11}Be, as a test case. The results show an important predictive power that opens a door to the understanding of other lesser known halo nuclei. In order to show the potential usefulness of the method, it is applied to analyze the structure of ^{19}C.

DOI: 10.1103/PhysRevC.89.014333 PACS number(s): 21.10.Jx, 21.60.−n, 24.10.Eq, 27.20.+n

I. INTRODUCTION

One of the main topics in nuclear physics during recent years is the study of nuclei far off the stability line. For these nuclei the ratio of protons to neutrons is quite different from the usual ratios for stable nuclei. Because of that, they are known as exotic nuclei. New physics is expected for these nuclei since, for instance, new close (sub)shells could appear affecting both the structure of the nucleus and its behavior when participating in nuclear reactions. Among the observed exotic nuclei, special interest has been devoted to halo nuclei. These are weakly bound systems composed by one or two weakly bound nucleons orbiting a relatively compact core. In the extreme weak-coupling limit, it is commonly assumed that the properties of this composite system are mainly determined by the degree of freedom of the weakly bound nucleon(s), commonly referred to as halo.

In this work we concentrate in two-body halo systems. In the simplest approach, the halo particle is assumed to move in a spherical mean-field potential generated by the remaining nucleons, leading to a description of the levels of the composite system in terms of single-particle orbitals. This simple picture is at the basis of many few-body reaction formalisms used in the analysis of reactions induced by halo and other weakly bound nuclei, such as the continuum-discretized coupled-channels (CDCC) method [1], the adiabatic approximation [2,3], the Faddeev/AGS equations [4,5], and a variety of semi-classical approaches [6–11]. Furthermore, in many of these applications, the valence-core potential is approximated by a simple phenomenological potential, with the parameters adjusted to reproduce the low-lying spectrum of the composite nucleus. This simple picture can be improved including some excited states of the core nucleus. These configurations are naturally included in microscopic approaches, such as the shell-model and *ab initio* approaches. Within an effective two-body Hamiltonian, these *core*-excited components are usually included assuming a collective model for the core nucleus (e.g., rotor or vibrator) giving rise to the so-called particle-rotor [12] or the particle-vibrator [13,14] models. In these models, in addition to the central potential, the valence-core interaction contains some non central term, which is responsible for the coupling between different core states and gives rise to core-excited admixtures in the states of the composite system. In practice, this is usually done by adding a transition potential with some phenomenological radial shape and a strength depending on some collective parameter. The parameters for the central and transition potentials are usually determined from the known properties of the composite system and, consequently, require some *a priori* knowledge of the properties of the system, such as the energy excitation and spin-parity assignment of the low-lying states. This restricts the predictive power of these models. Moreover, since the rotor and vibrator models are expected to be limiting cases, their accuracy is not guaranteed in specific cases.

To overcome these limitations, it would be desirable to construct a particle-plus-core model starting from more fundamental principles. Structure models based on microscopic many-body calculations are also potentially useful methods, but their applications to halo nuclei with a deformed core are still limited [15]. Alternatively, when some properties of the core nucleus are known (rms radius, excitation energies, etc.) one can make use of a semi-microscopic picture, and construct the interaction between the valence particle and the core nucleus by folding a suitable nucleon-nucleon effective interaction with an appropriate core density, following the same scheme used in the calculation of folding potentials for elastic and inelastic scattering [16].

It is our goal in this work to apply this idea to calculate the energies and wave functions of the states of one-neutron

*Present address: Dipartimento di Fisica e Astronomia, Università di Padova, I-35131 Padova, Italy; Istituto Nazionale di Fisica Nucleare, Sezione di Padova, I-35131 Padova, Italy; lay@us.es
†moro@us.es
‡ariasc@us.es
§yenyo@ruby.scphys.kyoto-u.ac.jp

halo nuclei. The aforementioned folding method is applied to generate the spin-independent part of the particle-core interaction. Both central and transition potentials are calculated within this scheme, making use of the appropriate monopole and transition densities. In the calculations presented in this work, the nucleon-nucleon interaction of Jeukenne, Lejeune, and Mahaux [17] is used as effective interaction, whereas the core densities are calculated here using the antisymmetrized molecular dynamics (AMD) method [18]. A phenomenological spin-orbit part, with standard parameters, is also added to the model Hamiltonian. It should be noted that the method can be equally applied with any other appropriate nucleon-nucleon interaction and/or different method to extract the core transition densities.

The paper is structured as follows. In Sec. II the particle-core Hamiltonian is defined and the method used to obtain the solutions (eigenfunctions and eigenenergies) of this Hamiltonian is explained. In Sec. III, the method is applied to ^{11}Be and ^{19}C. Finally, Sec. IV is devoted to discuss and summarize the main conclusions of this work.

II. CORE EXCITATIONS IN THE STRUCTURE OF TWO-BODY HALO NUCLEI

A. Particle-core model

We consider a composite nucleus, described as a two-body system, comprising a weakly-bound nucleon coupled to a core. In the weak-coupling limit, the Hamiltonian of the system can be written as

$$\mathcal{H} = h_{\rm core}(\xi) + T(\vec{r}) + V_{vc}(\vec{r},\xi), \tag{1}$$

where $T(\vec{r})$ is the kinetic energy operator for the relative motion between the valence and the core, $h_{\rm core}(\xi)$ is the Hamiltonian of the core, and $V_{vc}(\vec{r},\xi)$ is the effective valence-core interaction. The variable ξ denote the internal coordinates of the core. The dependence of $V_{vc}(\vec{r},\xi)$ on these coordinates account for core-excitation effects.

The eigenfunctions of this Hamiltonian, for a given energy ε, would be characterized by the total angular momentum $\vec{J}$, resulting from the coupling of the angular momentum $\vec{j}$ of the valence particle to the core angular momentum $\vec{I}$. These functions can be generically expressed as

$$\Psi_{\varepsilon;JM}(\vec{r},\xi) = \sum_{\alpha} R^{J}_{\varepsilon,\alpha}(r)[\mathcal{Y}_{(\ell s)j}(\hat{r}) \otimes \phi_I(\xi)]_{JM}, \tag{2}$$

where $\phi_I(\xi)$ denotes the core eigenstates, $\vec{\ell}$ is the orbital angular momentum between the valence particle and core, which couples to the spin of the valence particle ($\vec{s}$) to give the particle total angular momentum $\vec{j}$. The label α denotes the set of quantum numbers $\{\ell,s,j\}$. The radial functions $R^{J}_{\varepsilon,\alpha}(r)$ can be determined in several ways. A common procedure is to insert the expansion (2) into the Schrödinger equation, giving rise to a set of coupled differential equations for the radial functions $R^{J}_{\varepsilon,\alpha}(r)$ (see, e.g., [12]).

In this work, instead of this coupled-channels method, we use the so-called pseudo-state (PS) method. This method consists of diagonalizing the Hamiltonian in a finite basis of square integrable functions. This basis is chosen of the form

$$\phi^{THO}_{n,\alpha,J,M}(\vec{r},\xi) = R^{THO}_{n,\ell}(r)[\mathcal{Y}_{(\ell s)j}(\hat{r}) \otimes \phi_I(\xi)]_{JM} \tag{3}$$

where $R^{THO}_{n,\ell}(r)$ are a set of square-integrable radial functions. For the latter, we use the analytic transformed harmonic oscillator (THO) basis, which is obtained by applying a local scale transformation (LST) to the spherical HO basis as

$$R^{THO}_{n,\ell}(r) = \sqrt{\frac{ds}{dr}} R^{HO}_{n,\ell}[s(r)], \tag{4}$$

where $R^{HO}_{n,\ell}(s)$ (with $n = 1,2,\ldots$) is the radial part of the HO functions and $s(r)$ defines the LST. For the latter we use the analytical prescription of Karataglidis *et al.* [19]

$$s(r) = \frac{1}{\sqrt{2}b}\left[\left(\frac{1}{r}\right)^{m} + \left(\frac{1}{\gamma\sqrt{r}}\right)^{m}\right]^{-\frac{1}{m}}, \tag{5}$$

that depends on the parameters m and γ and the oscillator length b. In Ref. [19], it was stated that the LST depends very weakly on m and they suggested the value $m = 4$. In this work we adopt this value, so the only active parameters in the LST are b and γ. The ratio γ/b determines the range of the basis functions and the density of eigenstates as a function of the excitation energy: as γ decreases, the basis functions explore larger distances and the corresponding eigenvalues concentrate at lower excitation energies. Further details are given in Refs. [20,21].

The eigenstates of the Hamiltonian (1) will be expressed as an expansion in the THO basis, $\Phi^{(N)}_{i,J} = \sum_{n=1}^{N}\sum_{\alpha} C^{i}_{n,\alpha,J}\phi^{THO}_{n,\alpha,J}$, where N is the number of radial functions retained in the THO basis, i is an index labeling the eigenstates for a given J, and $C^{i}_{n,\alpha,J}$ are the expansion coefficients in the truncated basis. The negative eigenvalues of the Hamiltonian (1) are identified with the energies of the bound states, whereas the positive ones provide a discrete representation of the continuum spectrum. For small values of N, some of the positive-energy eigenvalues become stable with respect to small changes of N or of some nonlinear parameter of the basis (e.g., γ). These stabilized energies are identified with the resonances of the system [22,23].

B. Matrix elements of the Hamiltonian in the PS basis

The diagonalization of the Hamiltonian (1) requires the evaluation of the matrix elements of the potential V_{vc} in the PS basis, denoted in ket form as $|n(\ell s)jI;J\rangle$. For this purpose, it is convenient to separate the angular part by performing a multipole expansion of this interaction, i.e.,

$$V_{vc}(\vec{r},\xi) = \sum_{\lambda\mu} V_{\lambda\mu}(r,\xi)Y^{*}_{\lambda\mu}(\hat{r}) = \sum_{\lambda} V_{\lambda}(r,\xi)\cdot Y_{\lambda}(\hat{r}). \tag{6}$$

Then, following the convention for matrix elements used in Brink and Satchler [24], we obtain for each λ

$$\begin{aligned}\langle n(\ell s)jI;J||V_{\lambda}(r,\xi)\cdot Y_{\lambda}(\hat{r})||n'(\ell's)j'I';J\rangle \\ = (-1)^{(j'+I+J)}(2I+1)^{1/2}\langle n\ell I\|V_{\lambda}(r,\xi)\|n'\ell'I'\rangle \\ \times(2j+1)^{1/2}\begin{Bmatrix} j & j' & \lambda \\ I' & I & J\end{Bmatrix}\langle(\ell s)j\|Y_{\lambda}\|(\ell's')j'\rangle,\end{aligned} \tag{7}$$

where

$$\langle n\ell I\|V_\lambda(r,\xi)\|n'\ell' I'\rangle = \int dr\, r^2 R^{J*}_{n,\ell}(r) R^{J}_{n',\ell'}(r)\langle I\|V_\lambda(r,\xi)\|I'\rangle, \tag{8}$$

which contains the dependence of the assumed model for the core. For example, in the rotor model, these matrix elements read (see, e.g., [12,21,25,26])

$$\langle I||V_\lambda(r,\xi)||I'\rangle = V_\lambda(r)(-1)^{I-I'}\langle I K\lambda 0|I' K\rangle, \tag{9}$$

where K is the projection of the angular momentum on the core symmetry axis (usually $K=0$ for the lowest energy levels in even-even systems). Each $V_\lambda(r)$ reads

$$V_\lambda(r) = \int d\Omega\, V(r - R(\Omega))Y_{\lambda 0}(\theta,0), \tag{10}$$

$$R(\Omega) = R_0 + \sum_{\lambda\geqslant 2}\delta_\lambda Y_{\lambda 0}(\theta,0), \tag{11}$$

where usually we use a typical Woods-Saxon form for $V(r - R(\Omega))$ and only consider $\lambda = 0,2$, with $\delta_2 = \beta_2 R_0$ being the deformation length of the core.

C. Folding model for the valence-core interaction

In this work, we propose a simple semi-microscopic prescription, in which the $V_{vc}(\vec{r},\xi)$ interaction is calculated by means of a folding procedure, convoluting an effective in-medium NN interaction with microscopic transition densities of the core nucleus, i.e.,

$$V_{vc}(\vec{r},\xi) = \int d\vec{r'}\rho(\vec{r'},\xi)v_{nn}(\vec{r} - \vec{r'}). \tag{12}$$

where v_{nn} is the effective NN interaction and $\rho(\vec{r'},\xi)$ the density operator, defined as usual as

$$\rho(\vec{r},\xi) = \sum_{i=1}^{A}\delta(\vec{r} - \vec{r}_i). \tag{13}$$

This is conveniently expanded in multipoles as

$$\rho(\vec{r'},\xi) = \sum_{\lambda\mu}\rho_{\lambda\mu}(r',\xi)Y^*_{\lambda\mu}(\hat{r'}). \tag{14}$$

Note that, in the spherical case, $\rho(\vec{r'}) = \rho(r')$, and $V_{vc}(r)$ becomes a central potential, so it contains only the $\lambda = 0$ term. In a more general case, as we consider here, $\rho(\vec{r'},\xi)$ contains also noncentral terms that will give rise to transition terms with $\lambda > 0$ in the valence-core potential.

According to Eq. (7), one requires the reduced matrix elements of the V_{vc} interaction between different core states. In the folding scheme, these will be related to the matrix elements of the density operator between different core states, i.e.,

$$\begin{aligned}\langle I\nu|\rho(\vec{r},\xi)|I'\nu'\rangle &= \langle\phi_{I\nu}(\xi)|\sum_{i=1}^{A}\delta(\vec{r} - \vec{r}_i)|\phi_{I'\nu'}(\xi)\rangle \\ &= \sum_{\lambda,\mu}\langle I'\nu'\lambda\mu|I\nu\rangle\rho_{\lambda,I'\to I}(r)Y^*_{\lambda\mu}(\hat{r}),\end{aligned} \tag{15}$$

where $\rho_{\lambda,I'\to I}(r)$ correspond to the reduced matrix elements

$$\rho_{\lambda,I'\to I}(r) \equiv \langle I||\rho_\lambda||I'\rangle\,. \tag{16}$$

Our convention for reduced matrix elements is that of Brink and Satchler [24] so that the reversed densities are related as $\sqrt{2I'+1}\langle I'||\rho_\lambda||I\rangle = \sqrt{2I+1}\langle I||\rho_\lambda||I'\rangle$.

The density operator can be analogously defined for protons and neutrons ($\rho^{(p)}$ and $\rho^{(n)}$), in which case the sum in Eq. (13) runs over protons or neutrons, respectively. The corresponding monopole transition densities are normalized as

$$\int d\vec{r}\rho^{(p)}_{0,I\to I}(r)Y_{00}(\hat{r}) = Z, \tag{17}$$

$$\int d\vec{r}\rho^{(n)}_{0,I\to I}(r)Y_{00}(\hat{r}) = N. \tag{18}$$

For the proton case, the multipole terms are constrained by the electric transition probabilities, i.e.,

$$\mathcal{B}(E\lambda, I'\to I) = \frac{2I+1}{2I'+1}e^2\left|\int dr\, r^{\lambda+2}\rho^{(p)}_{\lambda,I'\to I}(r)\right|^2. \tag{19}$$

The core transition densities can be obtained with different methods. In this work, these densities are obtained from antisymmetrized molecular dynamics (AMD) [27,28] calculations for the core nucleus. This method is a microscopic structure model based on effective nuclear interactions in which the antisymmetrization between nucleons is fully taken into account. AMD wave functions are formed from Slater determinants of single-nucleon Gaussian wave functions. Namely, many-body wave functions are treated without assuming existence of any specific clusters in the method. Nevertheless, the AMD model space covers a variety of cluster structures and it can describe those of neutron-rich nuclei. Actually, the method has been proved to be very useful to understand the level structure and deformation of Be and B isotopes [18]. In the application to Be isotopes, it was shown that the structure of low-lying states can be described as two alpha clusters and remaining neutrons around the two alphas as proposed by Von Oertzen [29].

Following [16], the central part of the effective nucleon-nucleon interaction (v_{nn}) is decomposed in terms of the total spin (S) and isospin (T) of the colliding pair but, for simplicity, only the $S=0$ terms are considered,

$$v_{nn}(s) = v_{00}(s) + v_{01}(s)\vec{\tau'}\cdot\vec{\tau}\,, \tag{20}$$

where v_{ST} are the expansion terms and τ is the isospin operator. Attending to the isospin dependence, the v_{00} and v_{01} terms are called, respectively, isoscalar and isovector parts. The radial forms $v_{0T}(s)$ are taken from the work of Jeukenne, Lejeune, and Mahaux (JLM) [17],

$$v_{0T}(s,\rho,E) = \lambda_v V_T(\rho,E)(t_v\sqrt{\pi})^{-3}\exp\left(-s^2/t_v^2\right), \tag{21}$$

where the strength of the potential, V_T, depends on the density ρ, and the nucleon-nucleon relative energy E. In this case, for simplicity, we choose $E=0$. On the other hand, normalizations factors, λ_v, and the effective range of the Gaussian form factor, t_v, are adjustable parameters with typical values between 0.8 and 1.2 for λ_v, and between 1.2 and 1.4 for t_v. This interaction has been found to reproduce satisfactorily

the elastic and inelastic experimental cross sections in the intermediate energy region for light nuclei [30,31].

In order to evaluate Eq. (12) we also expand the interaction in multipoles as we did for the density:

$$v_{0T}(|\vec{r}-\vec{r}'|,\rho,E)=\sum_{\ell} v_{0T}^{(\ell)}(r,r')Y_{\ell}(\hat{r})\cdot Y_{\ell}(\hat{r}'). \qquad (22)$$

In the test cases considered in this work, the valence particle is a neutron, in which case the resulting potential can be expressed in terms of the corresponding proton and transition densities as [30]

$$\langle I||V_{\lambda}(r,\vec{\xi})||I'\rangle = \int dr' r'^2 \{ v_{00}^{(\lambda)}(r,r')\big[\rho_{\lambda,I'\to I}^{(n)}(r)+\rho_{\lambda,I'\to I}^{(p)}(r)\big] + v_{01}^{(\lambda)}(r,r')\big[\rho_{\lambda,I'\to I}^{(n)}(r')-\rho_{\lambda,I'\to I}^{(p)}(r')\big]\}. \qquad (23)$$

Note that, if the valence particle is a proton, the signs in the isovector part are changed.

III. APPLICATION TO HALO NUCLEI

A. Structure of ^{11}Be

As a test example of the formalism presented in the preceding section, we first consider the well known one-neutron halo nucleus ^{11}Be. Although the low-lying spectrum of this nucleus is reasonably described in terms of single-particle configurations, it is known that these states contain significant admixtures of core-excited components. To account for these components, within a particle-plus-core picture, several models have been used, such as the particle-vibrator (PVM) model [13,14] and the particle-rotor (PRM) model [32,33]. Pairing effects have also been treated approximately within the quasi-particle rotor (QPRM) and quasi-particle vibrator models (QPVM) [34].

Here, we compare the semi-microscopic approach proposed in this work with the particle-rotor model (PRM) developed by Nunes *et al.* [33,35] (model Be12-b). This model accounts well for the energies of the bound states and low-lying resonances $3/2^+_1$, $5/2^+_1$, and $3/2^-_1$ and has been previously employed to illustrate the use of the PS-THO basis described above [21].

The required transition densities in ^{10}Be are obtained from the antisymmetrized molecular dynamics (AMD) calculation of Ref. [27]. The AMD model is able to reproduce $E2$ transition probabilities between the different ^{10}Be energy levels with a substantial improvement with respect to the shell model calculations. In addition, the central and transition potentials calculated with these densities and the JLM potential are able to reproduce the $p+^{10}$Be inelastic cross sections at intermediate energies [31] within the distorted-wave Born approximation (DWBA) framework. This particle-core folding potential based in AMD transition densities will be referred to as P-AMD.

In our calculation, we will only consider valence configurations with $\ell \leqslant 2$ and the two lowest lying states in ^{10}Be, the 0^+ ground state and the 2^+ first excited state. All possible transition densities between these core states are plotted in Fig. 1. Convoluting the JLM interaction ($\lambda_v = 1.0$ and $t_v = 1.2$) with these densities, the potentials shown in Fig. 1 (right panels) are obtained. The $\rho_{0,2^+\to 2^+}$ density and the corresponding $\langle 2^+\|V_0\|2^+\rangle$ potential are included in the calculations although they are not plotted in Fig. 1. In the rotor model this potential coincides with the central $\langle 0^+\|V_0\|0^+\rangle$ one. In our P-AMD model both potentials are almost identical as so do the corresponding densities, confirming that the rotor assumptions are satisfied for the ^{10}Be core. The potentials have been calculated with the code MINC by M. Takashina [36].

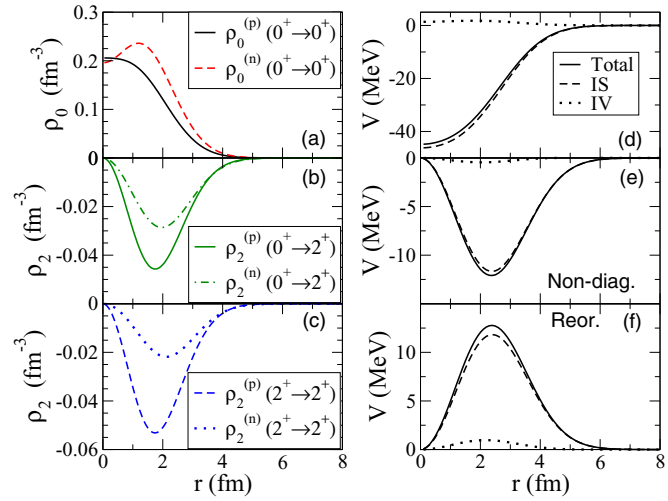

FIG. 1. (Color online) Neutron and proton transition densities for the two states considered in ^{10}Be, the 0^+ ground state and the 2^+ first excited state. The central densities, $\lambda = 0$, are shown in the upper-left panel normalized according to (18), and the quadrupole transition densities are shown in the lower-left panels. The corresponding transition potentials are shown in the right panels, with the isoscalar (IS) and isovector (IV) contributions indicated separately.

In addition to the central term, the n-^{10}Be interaction will contain spin-dependent parts. For simplicity, we consider only the spin-orbit term, for which we adopt the phenomenological parameterization of the potential Be12-b with a standard strength $V_{so} = 6$ MeV.

The calculated spectrum is shown in Fig. 2 (second column). Resonant energies are identified with stabilized eigenvalues with respect to variations in the number of states included in the THO basis [21]. The P-AMD calculation succeeds to produce two weakly bound states ($1/2^+$ and $1/2^-$), in agreement with experiment, but with the wrong ordering. Several low-lying resonances ($5/2^\pm$ and $3/2^\pm$) are also predicted. The inversion of the $1/2^+$ and $1/2^-$ levels has been ascribed to a combined effect of the core deformation, Pauli blocking, and pairing effects [14]. Pairing effects are completely ignored in our treatment whereas Pauli blocking is only considered approximately (see discussion below) so we cannot expect an accurate description of the experimental spectrum. To account in an effective way for these effects a slight renormalization of the folding potential is allowed. In order to reproduce the experimental ordering of the mentioned states, the renormalization factors need to be different for positive (λ_+) and negative (λ_-) parity states: $\lambda_+ = 1.054$ and $\lambda_- = 0.995$. The new spectrum is also shown in Fig. 2 (third column). The position of the resonances $3/2^-$, $5/2^+$,

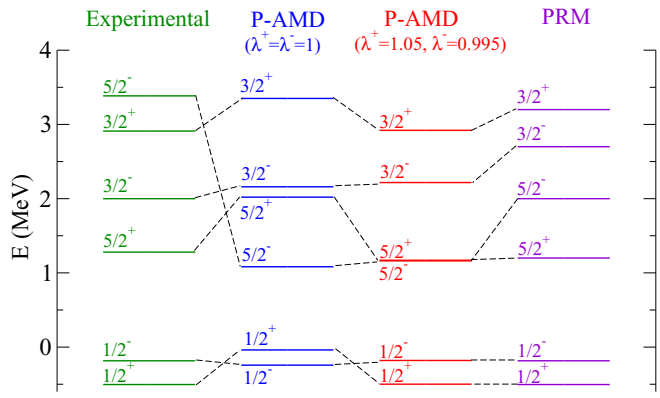

FIG. 2. (Color online) Experimental and calculated energy levels of ^{11}Be. Starting from the left, the second column is the P-AMD calculation without any renormalization. The third column is the P-AMD spectrum obtained with the indicated renormalization constants for positive (λ_+) and negative (λ_-) parity levels. The last column corresponds to the PRM calculation. Experimental values are from [37,38].

and $3/2^+$ are now reasonably well reproduced. Only the $5/2^-$ resonance is not well reproduced by the model. Considering that the only adjustable parameters are $\lambda_\pm$, and that the required normalizations are of the order of 5%, we can conclude that the overall agreement is fairly good. It is worth mentioning that the PRM model requires also a weaker strength for negative parity states to obtain the inversion. This fact can be related with the Pauli exclusion principle. The antisymmetrization of the wave functions should add an extra repulsion to $p_{1/2}$ configurations; repulsion that was added phenomenologically by reducing the strength of the negative parity potentials [39].

It is also worth noting that, in addition to the levels shown in Fig. 2, some other deeply bound eigenvalues are obtained in the diagonalization. These are identified with Pauli forbidden states and are therefore removed. These states come from the $1s_{1/2}$, $1p_{3/2}$, and $1p_{1/2}$ orbitals in the spherical basis, which are already occupied in the ^{10}Be nucleus according to our simple model in which exchange and pairing effects are ignored. By construction, the states obtained here are orthogonal to those removed, what should account for the Pauli principle. The forbidden states are therefore an admixture of different valence + core configurations. Note that, with this procedure, the part of the single-particle strengths of the $1s_{1/2}$, $1p_{3/2}$, and $1p_{1/2}$ orbitals will appear embedded among the retained valence + core states. Alternatively, the Pauli principle could be applied by removing these spherical valence configurations completely, as done for example in Refs. [40,41]. Both methods are indeed approximate. Since in the cases treated in this work the core is deformed, we follow the former approach. This election slightly affects the energies and spectroscopic factors obtained.

In Fig. 2, we can see that most of the low-lying structures in ^{11}Be can be understood within the P-AMD model. The spectra provided by P-AMD and PRM models [21] are compatible. P-AMD gives excitation energies for the positive parity resonances $5/2^+$ and $3/2^+$ in better agreement with experiment, although a major part of this effect is related to the spin-orbit term. P-AMD also improves the excitation energy for the negative parity resonance $3/2^-$.

TABLE I. Spectroscopic factors for the ground state and low-lying positive energy resonances in ^{11}Be, according to the different models considered.

	Model	$\|0^+\otimes(\ell s)j\rangle$	$\|2^+\otimes s_{1/2}\rangle$	$\|2^+\otimes d_{3/2}\rangle$	$\|2^+\otimes d_{5/2}\rangle$
$1/2^+$	PRM	0.857		0.021	0.121
	P-AMD	0.849		0.031	0.121
	WBT	0.762		0.002	0.184
$5/2^+$	PRM	0.702	0.177	0.009	0.112
	P-AMD	0.674	0.189	0.014	0.124
	WBT	0.682	0.177	0.009	0.095
$3/2^+$	PRM	0.165	0.737	0.017	0.081
	P-AMD	0.316	0.565	0.031	0.089
	WBT	0.068	0.534	0.008	0.167

In addition to the energies of the bound and resonant states, we have compared the weights of the various relevant components (channels) for the different models considered here. Within our assumed two-body model, these weights can be regarded as spectroscopic factors. In Table I these spectroscopic factors are shown for the positive parity states in ^{11}Be calculated for the P-AMD model, the particle-rotor model (PRM), and a shell model calculation with the WBT interaction from Warburton and Brown [42]. The latter was performed with the code OXBASH [43]. The three calculations give slightly different but compatible spectroscopic factors. In particular, these models agree in the dominance of the ^{10}Be(0^+) component for the ground state and $5/2^+$ resonance, as well as in the dominant ^{10}Be(2^+) contribution in the $3/2^+$ resonance.

The agreement between P-AMD and PRM values is not unexpected in view of the similarity of the corresponding transition potentials. These are shown in Fig. 3. The main difference is that the P-AMD densities yield a larger deformation of the core. In the PRM this deformation is a parameter that was estimated from the experimental quadrupole moment of the core, and corrected by the charge-to-mass deformation ratio given by shell model calculations [35]. On the other hand, a deformation parameter can be inferred from AMD densities comparing the transition density with the derivative of the central density. The relation between these two magnitudes, assuming that the rotor model is a good approximation, is

$$\rho_{\lambda,I'\to I}(r) \approx \langle I\|\hat{\delta}_\lambda\|I'\rangle \frac{d\rho_0}{dr}, \tag{24}$$

where $\langle I\|\hat{\delta}_\lambda\|I'\rangle$ is the reduced matrix element of the deformation length operator for a given transition. Multiplying in both sides by r^2 and integrating in r one obtains

$$\langle I\|\hat{\delta}_\lambda\|I'\rangle = \frac{1}{\lambda+2}\frac{\int \rho_{\lambda,I'\to I}(r) r^{\lambda+2} dr}{\int \rho_0(r) r^{\lambda+1} dr}. \tag{25}$$

Using the microscopic AMD densities employed in this work, one gets $\langle 0\|\hat{\delta}_2\|2\rangle_{\rm AMD} = 1.90$ fm. Interestingly, this value is very close to that obtained by Iwasaki *et al.* from a DWBA analysis of ^{10}Be(p,p') inelastic data, 1.80 ± 0.25 fm [44]. On the other hand, in the rotor model, these matrix elements are

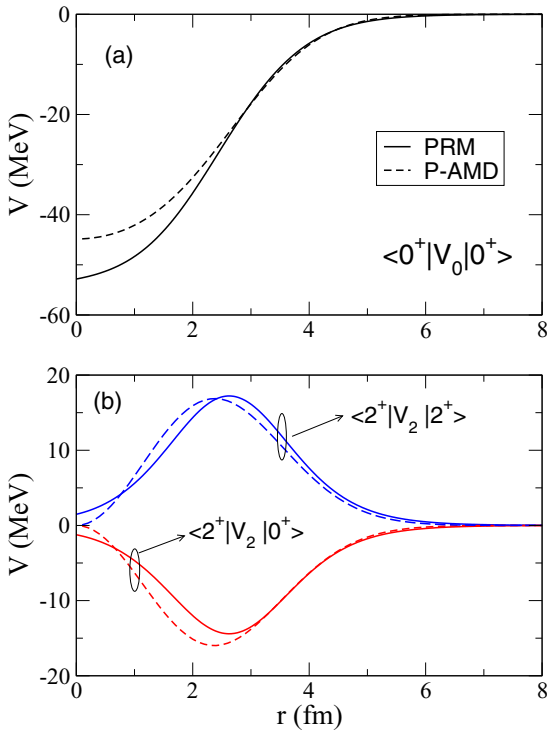

FIG. 3. (Color online) Potentials obtained for the n-^{10}Be system with the PRM model and with the P-AMD model. See text for details.

related to the intrinsic deformation as

$$\langle I \| \hat{\delta}_\lambda \| I' \rangle = \langle I K \lambda 0 | I' K \rangle \beta_\lambda R_0. \quad (26)$$

Inserting the mean radius and deformation parameter employed in our calculations ($R_0 = 2.483$ fm, $\beta_2 = 0.67$) one gets $\langle 0 \| \hat{\delta}_2 \| 2 \rangle_{\rm rot} = 1.66$ fm, which is somewhat smaller than the AMD value (these values are also listed in Table II for convenience). Consequently, the effective deformation obtained from the AMD densities is larger than that assumed in the rotor model used here, and this explains the larger mixing of the ^{10}Be(2^+) component in the ^{11}Be wave functions.

From the results presented in this subsection, we can conclude that the developed P-AMD model gives an overall good description of the bound states and low-lying resonances in ^{11}Be with very small adjustments of the parameters involved in the calculation. These results encourage us to use this model to make predictions for the structure of less well known halo nuclei. As an example, in the next subsection we apply the model to ^{19}C.

TABLE II. Properties of the ^{10}Be and ^{18}C systems, derived from the AMD and rotor calculations. The root-mean-square (rms) radius is obtained from the corresponding central AMD density.

Nucleus	rms radius (fm)	$\langle 0 \| \hat{\delta}_2 \| 2 \rangle_{\rm AMD}$ (fm)	$\langle 0 \| \hat{\delta}_2 \| 2 \rangle_{\rm rot}$ (fm)
^{10}Be	2.538	1.90	1.66[a]
^{18}C	2.776	1.20	1.50[b]

[a]Rotor model Be12-b of Ref. [33].
[b]Rotor model of Ref. [32], referred to in this work as PRM(1).

B. Structure of ^{19}C

After testing the semi-microscopic model with the well known nucleus ^{11}Be, we now consider the halo nucleus ^{19}C. The properties of this nucleus are not so well known, and the experimental data needed to adjust the parameters involved in phenomenological models (such as PRM or PVM) are scarce and, sometimes, contradictory. Therefore, a semi-microscopic model such as P-AMD can shed some light on the structure of this nucleus.

Although the properties of this nucleus, including the low-lying spectrum, are not well known, it has been recently the focus of several works [45–49]. It is known that the ground state has spin and parity $1/2^+$ and that the binding energy with respect to the ^{18}C + n threshold is 0.58 ± 0.09 MeV [50]. Almost all theoretical calculations predict $1/2^+$ (prolate) and $3/2^+$ (oblate) almost degenerate states [51]. In fact, the ground state spin and parity were not confirmed until recently [48]. The deformation for all lighter carbon isotopes is known to be prolate. For ^{19}C, prolate and oblate structures seem to be almost degenerate (shape coexistence), anticipating a kind of shape phase transition. It can be indicative of the presence of a new magic number, $N = 16$, for neutron-rich nuclei [51].

In addition to the $1/2^+$ and $3/2^+$ bound states, the analysis of the inelastic data of ^{19}C on protons reported in Ref. [52] suggested the existence of another bound excited state. This was assigned a spin-parity $5/2^+$ with the guidance of shell model calculations. Later on, in a exclusive breakup experiment of ^{19}C + p, a prominent peak was observed in the relative energy spectrum of the outgoing ^{18}C and n particles. Using microscopic DWBA calculations based on shell model densities, this state was associated with a second $5/2^+$ state predicted by some shell model calculations. This is the accepted experimental knowledge of the low-lying ^{19}C spectrum presented in the left part of Fig. 4. However, the experimental data are far from being clearly established. For

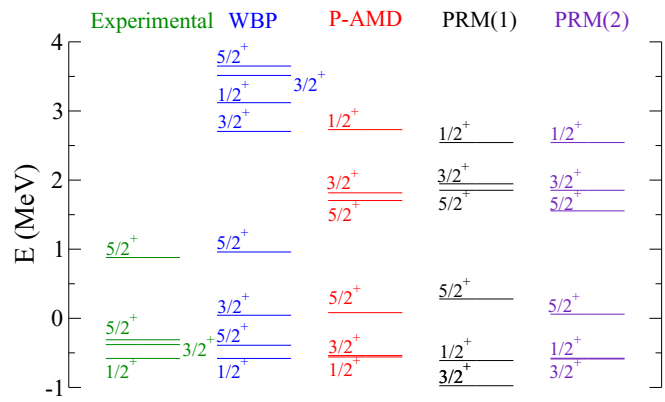

FIG. 4. (Color online) Spectrum obtained for the ^{19}C nucleus within the two PRM calculations [PRM(1) and PRM(2)], a shell model calculation (WBP), and with the single-folding calculation based on microscopic densities of the core (P-AMD) compared with the experimental one [48,52].

example, a recent knockout experiment [53] seems to question the existence of a $5/2^+$ bound state. From the theoretical point of view, the situation is also unclear. The quasi-particle rotor model (QPRM) of Ref. [34] gives correctly the $1/2^+$ ground state, but predicts that the first excited state is $5/2^+$. In Ref. [49], ^{19}C was studied within a multichannel algebraic method based upon a two-state, collective model for the $n + {}^{18}$C system. In order to reproduce the triplet of bound states reported by Elekes *et al.* [52] as well as the $5/2^+$ resonance suggested by Satou *et al.* [48] they need to introduce some Pauli hindrance of the $1d_{5/2}$ orbit. This introduces a phenomenological parameter in the model, which accounts for the amount of Pauli blocking of a given orbital. Clearly, the situation calls for further experimental and theoretical works.

With the aim of shedding some light into this problem, we present our prediction for the structure of ^{19}C within the semi-microscopic P-AMD framework. As in the ^{11}Be case, the neutron + ^{18}C folding potential was generated with the JLM nucleon-nucleon interaction, and the monopole and transition densities were calculated with AMD. These densities, and the corresponding transition potentials, are shown in Fig. 5. The central folded potential is supplemented with a phenomenological spin-orbit term, parameterized in terms of the derivative of a Woods-Saxon shape, with a standard strength $V_{so} = 6.5$ MeV. The geometry is adjusted to be consistent with the extension of the central part of the folding potential, obtaining $R_{so} = 3.0$ fm and $a_{so} = 0.70$ fm.

Diagonalizing the Hamiltonian, the spectrum shown under P-AMD in Fig. 4 is obtained. The experimental levels reported in Refs. [48,52], with the spin-parity assignment suggested in these works, are indicated in the left part of the figure. The prediction of two PRM calculations, labeled as PRM(1) and PRM(2), are shown at the right part of the figure. PRM(1) is from Tarutina and Hussein [32] that use a Woods-Saxon central potential with parameters $V_0 = -52.30$ MeV, $V_{so} = 6.5$ MeV, $R_0 = 3.0$ fm, and $a_0 = 0.65$ fm and a transition potential, obtained by deforming the central potential with a deformation parameter of $\beta_2 = 0.5$ fm. On the other hand, the model PRM(2) is obtained by adjusting the Wood-Saxon parameters to reproduce the potential provided by the P-AMD model. The aim of this PRM(2) model is to reproduce P-AMD results with simpler potentials in a more standard and widespread framework, so that these results can be more easily reproduced and used for different purposes. From this adjustment we obtained $V_0 = -51.80$ MeV, $R_0 = 3.0$ fm, and $a_0 = 0.70$ fm and assumed a deformation parameter $\beta_2 = 0.4$ fm. Also shown in Fig. 4 is the spectrum predicted by the shell model calculation performed with the WBP effective interaction of Warburton and Brown [42]. As expected, the PRM(2) model reproduces the P-AMD spectrum quite well.

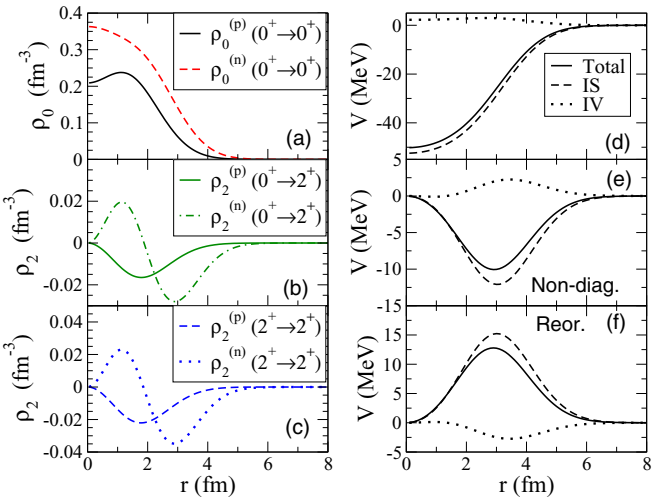

FIG. 5. (Color online) Neutron and proton transition densities between the two considered lowest lying states in ^{18}C, the 0^+ ground state and the 2^+ first excited state. The central densities, $\lambda = 0$, are shown in the upper-left panel normalized according to (18) and the quadrupole transition densities, in the lower-left panels. The corresponding transition potentials are shown in the right panels.

The P-AMD model predicts a $1/2^+$ ground state, with a separation energy of $S_n = -\varepsilon_{gs} = 0.582$ MeV, in excellent agreement with the experimental value. The first excited state is $3/2^+$, also in agreement with the experimental data, although in our model this state is almost degenerate with the ground state. No additional bound states are found in this model, contrary to the suggestions of [52]. The first resonant state is a $5/2^+_1$, which appears very close to the threshold. Taking into account the approximations implied in our model, one cannot rule out that this state is actually a weakly bound state, as suggested in [52]. A second $5/2^+$ resonance is obtained in P-AMD at $\varepsilon = 1.704$ MeV, but this state does not have a clear counterpart in the experimental spectrum. No states are found close to the resonant peak observed by Satou *et al.* [48] which, again, could be attributed to the uncertainties of our model. The PRM(1) model predicts also two bound states with spin and parity $1/2^+$ and $3/2^+$, but with the latter being lower in energy. As in the P-AMD model, the second $5/2^+$ state appears as a low-lying resonance close to the neutron separation threshold.

The transition potentials obtained with the P-AMD, PRM(1) and PRM(2) models are compared in Fig. 6. The central potentials are similar in the three models, whereas the quadrupole transition potentials ($\langle 2^+ \| V_2 \| 2^+ \rangle$ and $\langle 2^+ \| V_2 \| 0^+ \rangle$) are larger in the PRM(1) model. This can be understood in terms of the corresponding deformation lengths. The values computed with Eqs. (25) and (26) are listed in Table II. In this case, the deformation predicted by the AMD model is smaller than the one assumed in the rotor model PRM(1), and this explains the stronger transition potential in the latter case.

Despite slight disagreements in energy, all studied models give the same spin and parity for the four lowest-lying states. In Table III the spectroscopic factors provided by the different models for these four levels are presented. Good agreement is found for all the states as in ^{10}Be. In the case of the two $5/2^+$ states, the ordering predicted by the PRM and P-AMD models seems to be inverted with respect to the shell model prediction.

It is worth mentioning that the original value of the central potential depth in model PRM(1) was $V_0 = -42.95$ MeV [32]. With this choice one obtains, a $1/2^+$ state with the experimental separation energy and a deeply bound $1/2^+$ state, which is considered to be Pauli forbidden. In the calculations presented in this work, we assume that there is

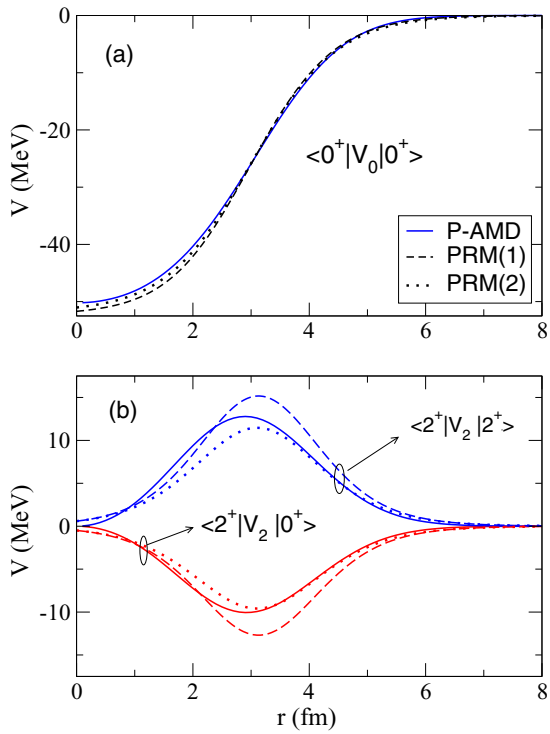

FIG. 6. (Color online) Potentials obtained for the n-^{18}C system with the PRM and P-AMD models.

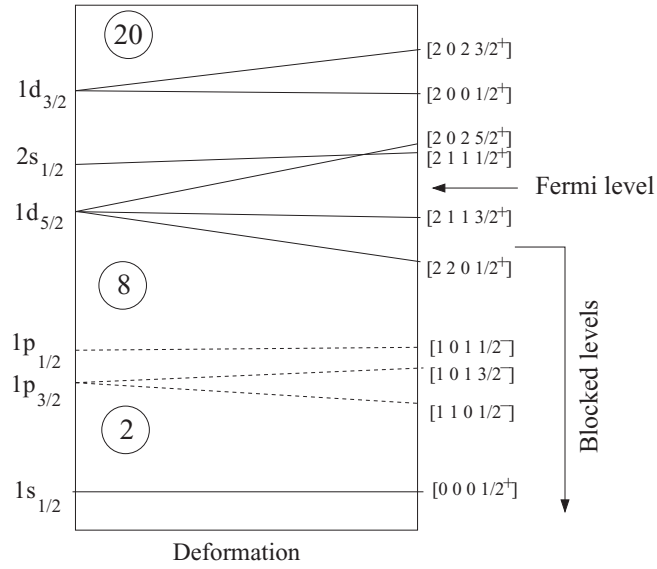

FIG. 7. Schematic diagram for the lowest Nilsson levels relevant for the calculation of the Pauli forbidden states in our P-AMD model for ^{19}C.

an additional $1/2^+$ Pauli forbidden state, and hence the depth of the potential has been increased accordingly in order the third $1/2^+$ eigenvalue has the experimental separation energy. The last neutrons in ^{18}C partially occupy the $2s_{1/2}$ and $1d_{5/2}$ orbits, so that full removal of these spherical configurations may produce misleading results. In order to estimate the number of Pauli forbidden states we follow the procedure of Ref. [54], which makes use of the strong coupling limit in the simple Nilsson model [12,54]. Using the asymptotic quantum numbers $[Nn_z\Lambda K^\pi]$, corresponding to large prolate deformations, the relevant Nilsson levels for ^{18}C ($N = 12$) are $[000\frac{1}{2}^+]$, $[110\frac{1}{2}^-]$, $[101\frac{3}{2}^-]$, $[101\frac{1}{2}^-]$, $[220\frac{1}{2}^+]$, $[211\frac{3}{2}^+]$, $[211\frac{1}{2}^+]$, and $[202\frac{5}{2}^+]$ (see the scheme in Fig. 7). In this extreme model the occupancy of each level is 2. Levels well below the Fermi level are completely occupied and blocked; levels around the Fermi level are only partially occupied and participate in the low-energy excitation of the system. In the ^{18}C case the five lowest Nilsson levels are fully occupied and blocked. The extra two neutrons of the core can occupy partially $[211\frac{3}{2}^+]$, $[211\frac{1}{2}^+]$, and $[202\frac{5}{2}^+]$ but do not block completely these levels for the extra neutron in ^{19}C. In order to calculate the Pauli forbidden states for the extra neutron, $[000\frac{1}{2}^+]$, $[110\frac{1}{2}^-]$, $[101\frac{3}{2}^-]$, $[101\frac{1}{2}^-]$, and $[220\frac{1}{2}^+]$ levels are blocked. Taking into account that we are only interested in positive parity states in ^{19}C, and that we are including only the 0^+ and the first excited state 2^+ states of the core, the negative parity Nilsson orbitals are not important since they will produce negative parity states in ^{19}C. Consequently, the relevant blocked Nilsson levels are $[000\frac{1}{2}^+]$ and $[220\frac{1}{2}^+]$. The Nilsson model corresponds to an adiabatic approximation of the particle-core model in which the core states are assumed to be degenerate in energy. Once the energy of the core states is increased the K quantum number is no longer a good quantum number, but one can monitor how the orbits characterized by this quantum number splits into several nondegenerate states, characterized by the total angular momentum J of the system. In particular, one gets two $1/2^+$ states ($1/2^+ \otimes 0^+$ from $[000\frac{1}{2}^+]$ and $[220\frac{1}{2}^+]$), two $3/2^+$ states, and two $5/2^+$ states ($1/2^+ \otimes 2^+$ from $[000\frac{1}{2}^+]$ and $[220\frac{1}{2}^+]$) that should be removed. Thus, in our calculations, the third $1/2^+$ state is

TABLE III. Spectroscopic factors for the ground state and low-lying positive energy resonances in ^{19}C, according to the different models considered in this work.

	Model	$\|0^+ \otimes (\ell s) j\rangle$	$\|2^+ \otimes s_{1/2}\rangle$	$\|2^+ \otimes d_{3/2}\rangle$	$\|2^+ \otimes d_{5/2}\rangle$
$1/2^+_1$	P-AMD	0.529		0.035	0.436
	PRM(1)	0.517		0.081	0.402
	PRM(2)	0.505		0.033	0.462
	WBP	0.580		0.085	0.470
$3/2^+_1$	P-AMD	0.028	0.386	0.121	0.464
	PRM(1)	0.043	0.348	0.150	0.459
	PRM(2)	0.023	0.371	0.106	0.500
	WBP	0.026	0.494	0.001	0.076
$5/2^+_1$	P-AMD	0.276	0.721	0.000	0.003
	PRM(1)	0.285	0.716	0.000	0.003
	PRM(2)	0.278	0.719	0.000	0.003
	WBP	0.383	0.015	0.000	0.751
$5/2^+_2$	P-AMD	0.200	0.142	0.002	0.657
	PRM(1)	0.217	0.178	0.004	0.602
	PRM(2)	0.207	0.100	0.002	0.690
	WBP	0.035	0.609	0.009	0.291

considered to be the physical ground state of the ^{19}C system. The fact that, with this selection of Pauli forbidden states, the ground state energy, its spectroscopic factor, and the level scheme, among other observables, are in good agreement with experimental data and shell model calculations as shown in Table III and Fig. 4 supports this procedure of calculating the Pauli forbidden states.

IV. SUMMARY AND CONCLUSIONS

A semi-microscopic particle-plus-core description of one-neutron halo nuclei, considering excitations of the core, has been presented. In this model, the neutron-core interaction is constructed by folding an effective nucleon-nucleon interaction with microscopic (monopole and transition) densities of the core. For the former, the JLM [17] interaction is chosen, whereas the densities are calculated with the anti-symmetrized molecular dynamics (AMD) method. The folded potential is supplemented with a phenomenological spin-orbit interaction.

The model has been applied to the well known halo nucleus ^{11}Be (^{10}Be + n) and to the less known halo nucleus ^{19}C (^{18}C + n). In the ^{11}Be case, the model is able to reproduce the experimental spectrum using standard parameters for the JLM interaction in the region of the nucleus. Small normalization factors, different for positive and negative parity states, are required in order to reproduce the separation energies of the two bound states in ^{11}Be. However, these normalization factors are close to 1 ($\lambda_+ = 1.056$ and $\lambda_- = 0.995$ for positive and negative parity states, respectively) suggesting that this semi-microscopic description can have predictive power to study less known nuclei with an important effect of core excitations, such as odd-even nuclei in deformed regions. The small difference in the renormalization factors can be understood considering the effect of Pauli repulsion in the negative parity states due to the nucleons that fill the $1p_{3/2}$ and $1p_{1/2}$ states. The good agreement between the spectroscopic factors from particle-rotor model, shell model, and this semi-microscopic description also supports the predictive power of this method.

Based on these results, AMD densities for ^{18}C [28] have been used to obtain the spectrum, spectroscopic factors and properties of the ^{19}C nucleus. Very few experimental data are available for this halo nucleus. Without any renormalization of the coupling potentials, the model reproduces the spin-parity ($1/2^+$) and the separation energy ($S_n = 0.58$ MeV) of the ground state. It also predicts the existence of a bound $3/2^+$ state, in agreement with shell model calculations and experimental evidence. Two low-lying $5/2^+$ resonances have been found. The calculated spectroscopic factors for these two resonances suggest a possible inversion in the energy sequence of these states with respect to the shell model. Apart from this exception, it should be emphasized that the proposed semi-microscopic model is able to reproduce an important part of the available experimental data for ^{11}Be and ^{19}C.

The predictive power of the model makes it particularly useful for exotic nuclei for which scarce information is available, such as ^{19}C and other unknown nuclei. Although we compare with particle-rotor models, the proposed model does not need the core to be either a rotor or a vibrator. That makes the model far more general and suitable for different regions of exotic nuclei. Whenever we have a certain knowledge of the core, the model can be used to predict the spectrum of the core+neutron (or core+proton) composite system. Furthermore, since it uses the same THO formalism as the PRM model used in [55], it will be easily included in reaction calculations including core excitations, as we hope to show in future works.

An important issue for extending the application of this model would be the correct application of the Pauli principle. Here we have removed those final deeply bound eigenstates that we considered as occupied by comparing with the spherical and Nilsson limits for each case. Differences between removing these eigenstates, removing pure spherical or Nilsson configurations, and more sophisticated treatments of the Pauli principle should lead to future developments of the present model.

In this work, a particular nucleon-nucleon interaction (JLM) and method to extract core transition densities (AMD) have been used. However, the formalism proposed is general and is not linked to them. It can be equally applied with any other appropriate NN interaction and/or model able to calculate core transition densities.

ACKNOWLEDGMENTS

This work has been partially supported by the Spanish Ministerio de Ciencia e Innovación and FEDER funds under projects FIS2011-28738-c02-01, FPA2009-07653, FPA2009-08848, by the Spanish Consolider-Ingenio 2010 Programme CPAN (CSD2007-00042) and by Junta de Andalucía (FQM160, P11-FQM-7632). J.A.L. acknowledges a research grant by the Ministerio de Ciencia e Innovación.

[1] N. Austern, Y. Iseri, M. Kamimura, M. Kawai, G. Rawitscher, and M. Yahiro, Phys. Rep. **154**, 125 (1987).
[2] P. Banerjee and R. Shyam, Phys. Rev. C **61**, 047301 (2000).
[3] J. A. Tostevin, S. Rugmai, and R. C. Johnson, Phys. Rev. C **57**, 3225 (1998).
[4] L. D. Faddeev, Zh. Eksp. Theor. Fiz. **39**, 1459 (1960) [Sov. Phys. JETP **12**, 1014 (1961)].
[5] E. O. Alt, P. Grassberger, and W. Sandhas, Nucl. Phys. B **2**, 167 (1967).
[6] S. Typel and G. Baur, Phys. Rev. C **50**, 2104 (1994).
[7] H. Esbensen and G. F. Bertsch, Nucl. Phys. A **600**, 37 (1996).
[8] T. Kido, K. Yabana, and Y. Suzuki, Phys. Rev. C **50**, R1276 (1994).
[9] S. Typel and G. Baur, Phys. Rev. C **64**, 024601 (2001).
[10] P. Capel, G. Goldstein, and D. Baye, Phys. Rev. C **70**, 064605 (2004).
[11] A. Garcia-Camacho, A. Bonaccorso, and D. M. Brink, Nucl. Phys. A **776**, 118 (2006).

[12] A. Bohr and B. Mottelson, Nuclear Structure (W. A. Benjamin, New York, 1969).
[13] N. Vinh Mau, Nucl. Phys. A **592**, 33 (1995).
[14] G. Gori, F. Barranco, E. Vigezzi, and R. A. Broglia, Phys. Rev. C **69**, 041302 (2004).
[15] P. Descouvemont and M. S. Hussein, Phys. Rev. Lett. **111**, 082701 (2013).
[16] G. Satchler and W. Love, Phys. Rep. **55**, 183 (1979).
[17] J. P. Jeukenne, A. Lejeune, and C. Mahaux, Phys. Rev. C **16**, 80 (1977).
[18] Y. Kanada-Enyo, H. Horiuchi, and A. Ono, Phys. Rev. C **52**, 628 (1995); Y. Kanada-Enyo and H. Horiuchi, *ibid*. **52**, 647 (1995).
[19] S. Karataglidis, K. Amos, and B. G. Giraud, Phys. Rev. C **71**, 064601 (2005).
[20] J. A. Lay, A. M. Moro, J. M. Arias, and J. Gomez-Camacho, Phys. Rev. C **82**, 024605 (2010).
[21] J. A. Lay, A. M. Moro, J. M. Arias, and J. Gómez-Camacho, Phys. Rev. C **85**, 054618 (2012).
[22] A. U. Hazi and H. S. Taylor, Phys. Rev. A **1**, 1109 (1970).
[23] J. A. Lay, J. M. Arias, J. Gómez-Camacho, and A. M. Moro, *Beauty in Physics: Theory and Experiment*, May 2012, Hacienda Cocoyoc, Mexico, edited by R. Bijker, AIP Conf. Proc. No. 1488 (AIP, New York, 2012), p. 436.
[24] D. M. Brink and G. R. Satchler, *Angular Momentum* (Clarendon, Oxford, 1968).
[25] T. Tamura, Rev. Mod. Phys. **37**, 679 (1965).
[26] I. J. Thompson and F. M. Nunes, *Nuclear Reactions for Astrophysics* (Cambridge University Press, Cambridge, 2009).
[27] Y. Kanada-En'yo, H. Horiuchi, and A. Doté, Phys. Rev. C **60**, 064304 (1999).
[28] Y. Kanada-En'yo, F. Kobayashi, and T. Suhara, J. Phys. Conf. Ser. **436**, 012037 (2013); **445**, 012037 (2013).
[29] W. von Oertzen, Z. Phys. A **354**, 37 (1996).
[30] M. Takashina, Y. Kanada-En'yo, and Y. Sakuragi, Phys. Rev. C **71**, 054602 (2005).
[31] M. Takashina and Y. Kanada-En'yo, Phys. Rev. C **77**, 014604 (2008).
[32] T. Tarutina and M. S. Hussein, Phys. Rev. C **70**, 034603 (2004).
[33] F. Nunes, J. Christley, I. Thompson, R. Johnson, and V. Efros, Nucl. Phys. A **609**, 43 (1996).
[34] T. Tarutina, A. R. Samana, F. Krmpotic, and M. S. Hussein, Braz. J. Phys. **36**, 1349 (2006).
[35] F. Nunes, I. Thompson, and R. Johnson, Nucl. Phys. A **596**, 171 (1996).
[36] M. Takashina, single-folding model code MINC (private comunication).
[37] N. Fukuda *et al*., Phys. Rev. C **70**, 054606 (2004).
[38] Y. Hirayama, T. Shimoda, H. Izumi, A. Hatakeyama, K. P. Jackson, C. D. P. Levy, H. Miyatake, M. Yagi, and H. Yano, Phys. Lett. B **611**, 239 (2005).
[39] F. Nunes, Ph.D. thesis, University of Surrey, 1995 (unpublished).
[40] V. Kukulin, V. Krasnopol'sky, V. Voronchev, and P. Sazonov, Nucl. Phys. A **453**, 365 (1986).
[41] T. Myo, K. Kato, H. Toki, and K. Ikeda, Phys. Rev. C **76**, 024305 (2007).
[42] E. K. Warburton and B. A. Brown, Phys. Rev. C **46**, 923 (1992).
[43] B. A. Brown, A. Etchegoyen, and W. D. M. Rae, MSU-NSCL Report No. 524, 1986 (unpublished).
[44] H. Iwasaki *et al*., Phys. Lett. B **481**, 7 (2000).
[45] S. Typel and R. Shyam, Phys. Rev. C **64**, 024605 (2001).
[46] T. Nakamura *et al*., Phys. Rev. Lett. **83**, 1112 (1999).
[47] I. Hamamoto, Phys. Rev. C **76**, 054319 (2007).
[48] Y. Satou *et al*., Phys. Lett. B **660**, 320 (2008).
[49] S. Karataglidis, K. Amos, P. Fraser, L. Canton, and J. Svenne, Nucl. Phys. A **813**, 235 (2008).
[50] G. Audi, A. H. Wapstra, and C. Thibault, Nucl. Phys. A **729**, 337 (2003).
[51] T. Suzuki, H. Sagawa, and K. Hagino, Phys. Rev. C **68**, 014317 (2003).
[52] Z. Elekes *et al*., Phys. Lett. B **614**, 174 (2005).
[53] N. Kobayashi *et al*., Phys. Rev. C **86**, 054604 (2012).
[54] Y. Urata, K. Hagino, and H. Sagawa, Phys. Rev. C **83**, 041303 (2011).
[55] A. M. Moro and J. A. Lay, Phys. Rev. Lett. **109**, 232502 (2012).